


Stability and formation of hydroxylated α -Al₂O₃(0001) surfaces at high temperaturesJiachen Chen , Dmitry Sharapa , and Philipp N. Plessow **Institute of Catalysis Research and Technology, Karlsruhe Institute of Technology, Hermann-von-Helmholtz Platz 1, 76344 Eggenstein-Leopoldshafen, Germany*

(Received 29 December 2021; accepted 27 February 2022; published 28 March 2022)

We report a type of termination of the α -Al₂O₃(0001) surface with low concentration of hydroxyl groups. Using density functional theory calculations, we show that this termination is more stable than previously reported structures for low chemical potentials of water. This means that hydroxyl groups remain thermodynamically stable up to much higher temperatures than predicted previously, for example, up to around 1000 K at 1 mbar partial pressure of water. We also study the formation of these hydroxylated surfaces from adsorbed water and show that the initial steps for surface reconstruction are favorable thermodynamically and also proceed with accessible barriers.

DOI: [10.1103/PhysRevResearch.4.013232](https://doi.org/10.1103/PhysRevResearch.4.013232)

I. INTRODUCTION

The α -Al₂O₃(0001) surface is frequently studied, for example, with respect to its interface with solids and liquids [1–14]. Like γ -alumina [15], α -alumina is also employed as a support material for metal particles in catalysis [16–28] and for atoms or molecules [29–33]. The level of hydroxylation has been shown to critically influence the reactivity of oxide surfaces [34–40]. Due to its importance, multiple studies have also focused on the atomic structure of the clean α -Al₂O₃(0001) surface itself [41–43]. However, many aspects remain unclear, such as, specifically, how the surface termination changes as a function of external conditions.

In ultrahigh vacuum (UHV), the clean (1 × 1)- α -Al₂O₃(0001) surface is stable until, at temperatures higher than 1000 °C, surface reconstructions take place. Most notably, at above 1350 °C, the oxygen-deficient ($\sqrt{31} \times \sqrt{31}$)R9° surface is formed [44–48]. The hydroxylated state of the α -Al₂O₃(0001) surface, which is caused by exposure to water, has also received considerable attention [49]. Based on temperature-programmed-desorption (TPD) experiments, it has been concluded that water is completely desorbed at temperatures higher than 600 K [50]. On the other hand, analysis of x-ray photoelectron spectroscopy (XPS) of the O 1s level suggests that hydroxyl groups are present even when the surface is annealed up to 1000–1200 K [34,35]. Different reports, however, propose that characteristic high-temperature XPS features do not stem from OH groups [51]. Based on

ion-scattering experiments, it was concluded that OH groups are present up to 1100 °C [52]. The use of low-energy electron diffraction (LEED) for structure determination is limited because the electron beam has been reported to lead to dehydroxylation [44,53]. The presence of water was also studied for the α -Al₂O₃(1 $\bar{1}$ 02) surface [54,55], for the α -Al₂O₃(11 $\bar{2}$ 0) surface [55–59], and for other modifications of Al₂O₃, such as the γ and θ phases [60–63].

Various theoretical investigations have shown that the Al-terminated, stoichiometric (1 × 1) surface is the most stable α -Al₂O₃(0001) surface in the absence of water and that the formation of reduced surfaces is expected only for low chemical potentials of oxygen [64,65]. Two main types of hydroxylated surfaces have been studied theoretically. The first surface results from water adsorption and dissociation on the clean surface [66–73]. Here, multiple investigations have shown that water adsorption and dissociation are facile up to $\mu_{\text{H}_2\text{O}} \approx -1.5$ eV. The barrier for dissociation was shown to be low, < 0.5 eV [67,70], and further diffusion of the dissociated proton was also studied [69,74]. Another termination is the fully hydroxylated surface, which can be derived from the oxygen-terminated α -Al₂O₃(0001) surface, where every surface oxygen is saturated with a hydrogen. This results in the most stable known hydroxylated surface [64,67,68]. At low temperatures, an additional two-dimensional (2D)-ice-like layer of water was predicted to form on top of this surface, and this has also been investigated in detail [66–68,75,76]. Despite being more stable, it is not clear how the fully hydroxylated surface can form from the stoichiometric surface, since these surfaces differ in the concentration of Al atoms in the first layer [66,68].

In this paper, we employ density functional theory (DFT) calculations to study the stability and the formation mechanism of hydroxylated α -Al₂O₃(0001) surfaces. First, we show that more stable structures than previously predicted exist, which can be described as Al(OH)₃ adsorbed with low coverage on the stoichiometric surface. After that, we study the mechanism for the formation of these surfaces starting from

*plessow@kit.edu

Published by the American Physical Society under the terms of the [Creative Commons Attribution 4.0 International license](https://creativecommons.org/licenses/by/4.0/). Further distribution of this work must maintain attribution to the author(s) and the published article's title, journal citation, and DOI.

the well-known water adsorption and dissociation on the dry surface.

II. METHODS

All DFT calculations were performed using the projector-augmented wave (PAW) method, standard PAW potentials, and a kinetic energy cutoff of 400 eV for the expansion of the wave function in plane waves. The calculations were carried out with version 5.4.1 of the Vienna *ab initio* simulation package (VASP), except for calculations with the strongly constrained and appropriately normed functional (SCAN) [77], which were done with version 5.4.4 [78,79]. All calculations use real-space projectors (“LREAL=AUTO” in VASP) and a plane-wave basis set for the electronic density, which includes reciprocal lattice vectors with a norm up to 3/2 times larger than that for the wave function, $|\mathbf{G}_{\text{cut}}|$ (“PREC=Normal” in VASP). All optimizations and the main results in this paper were obtained with the Perdew-Burke-Ernzerhof (PBE) [80] functional and Grimme’s D3 dispersion correction [81]. Other density functionals (the Bayesian error estimation functional with van der Waals correlation (BEEF-vdW) [82], SCAN [77], and the 2006 Heyd-Scuseria-Ernzerhof functional (HSE-06) [83,84]) were also tested. A self-consistent field (SCF) convergence criterion of $< 10^{-8}$ eV was used for the total energy, and a geometry convergence criterion of < 0.01 eV/Å was used for the maximum norm of individual atomic forces. The lattice constants of α -Al₂O₃ were optimized using an increased cutoff of 800 eV, and the obtained values ($a = b = 4.787$ Å, $c = 13.045$ Å) agree well with the experiment ($a = b = 4.763$ Å, $c = 13.003$ Å) [18].

Surfaces were modeled as slabs with 7 f.u. of Al₂O₃ per stoichiometric (1 × 1) surface and slabs of corresponding thickness for other terminations. The lower part of the slabs was terminated by a single Al layer (stoichiometric termination), and the bottom Al₇O₉ unit per (1 × 1) surface were kept frozen at their bulk positions. The slabs were separated by at least 16 Å of vacuum to prevent artificial interaction between periodic images. The Brillouin zone of surfaces was sampled using a Γ -centered k -point grid with a density corresponding to at least (3 × 3 × 1) per (1 × 1)- α -Al₂O₃(0001) cell and using Gaussian smearing with $\sigma = 0.1$ eV.

The stability of all surfaces is discussed in terms of the surface free energy γ , which is computed as the Gibbs free energy of formation relative to the dry surface, per surface area A :

$$\gamma = \frac{E^{\text{slab}} - E_{\text{dry}}^{\text{slab}} - \frac{n}{2} E_{\text{Al}_2\text{O}_3}^{\text{bulk}} - m[E_{\text{H}_2\text{O}}^{\text{gas}} + \mu_{\text{H}_2\text{O}}]}{A}. \quad (1)$$

Here, E^{slab} and $E_{\text{dry}}^{\text{slab}}$ are the energies of the slab models of the considered surface and of the dry surface with identical surface area A , and $E_{\text{Al}_2\text{O}_3}^{\text{bulk}}$ is the energy per formula unit of bulk α -Al₂O₃. The surface area per (1 × 1) cell is $A = 19.845$ Å². The energy per bulk formula unit $E_{\text{Al}_2\text{O}_3}^{\text{bulk}}$ was determined as the energy difference between two clean (1 × 1) slabs differing by one Al₂O₃ layer, and this energy was used in all calculations. Calculating the same energy difference $E_{\text{Al}_2\text{O}_3}^{\text{bulk}}$ for other unit cells or terminations led to negligible differences of the order of 0.001 eV. The chemical potential of water $\mu_{\text{H}_2\text{O}}$ is given relative to the energy of water $E_{\text{H}_2\text{O}}^{\text{gas}}$ and is generally

a function of temperature and partial pressure. The stoichiometry coefficients n and m are determined by the amount of additional Al and H atoms on the surface with respect to the dry surface.

Reaction paths were optimized using a (3 × 3) cell with (1 × 1) k -point sampling, which is smaller than the (2 × 2) k -point sampling used to compute the thermodynamic stability of (3 × 3) surfaces. This is justified because formation energies per (3 × 3) cell computed with the smaller k -point sampling differ by less than 0.01 eV (total energies differ by 0.03 eV). The highest barriers of each pathway were determined explicitly, i.e., the transition states were obtained as stationary points with a maximum atomic force component of 0.01 eV/Å, and it was furthermore verified that they are first-order saddle points through calculation of a partial Hessian matrix, which gives a single imaginary frequency in normal mode analysis. The connectivity of the transition state was additionally verified through small displacements along the transition mode followed by optimization to the end points. Transition states were optimized either using constraints [85] or using the dimer method [86]. Lower barriers were in some cases only estimated through nudged elastic band (NEB) calculations [87], which use typically 10–15 images. Additional images were added through linear interpolation in Cartesian space, so that the norm of the distance between the images in Cartesian coordinates is always < 0.1 Å. This results in a dense reaction path with typically 50–150 images that provides a rigorous upper limit to the exact barrier. Energies and optimized structures are provided in the Supplemental Material [88].

III. RESULTS AND DISCUSSION

A. Thermodynamic stability of hydroxylated surfaces

The bulk structure of α -Al₂O₃ can be described as a hexagonal AB stacking of close-packed O²⁻ ions in the 0001 direction, with Al³⁺ occupying two-thirds of the available octahedral positions. The unit cell consists of three O²⁻ ions per layer and two Al³⁺ ions in between (see Fig. 1). The Al³⁺ ions form ABC layers, in which the unoccupied octahedral position alternates between the three possible locations. This means that the two Al³⁺ ions per layer are not equivalent and are slightly distorted in the 0001 direction. The Al layering can be described as an (-O₃-Al₂-) stacking, and because of the AB stacking of O²⁻ and the ABC stacking of Al³⁺, a total of six (O₃-Al₂) layers make up the unit cell; see Fig. 1. In agreement with previous work [41,89,90], we find that the most stable stoichiometric surface is a (1 × 1) surface that is terminated by a single Al layer (O₃-Al), which is relaxed inwards considerably: -88% predicted by DFT, -63% determined by LEED [52], and -51% determined by x-ray diffraction (XRD) [91,92].

Figure 1 shows the most important known hydroxylated structure, the Al₂-(OH)₃-terminated (gibbsite-like) surface [64,67,68]. This surface is terminated by a full layer of oxygen that is saturated with one hydrogen per oxygen giving an OH concentration of 3 per (1 × 1) cell or 15.1 per nm². Based on XRD, the structure of α -Al₂O₃(0001) at room temperature and ambient pressure has been assigned to

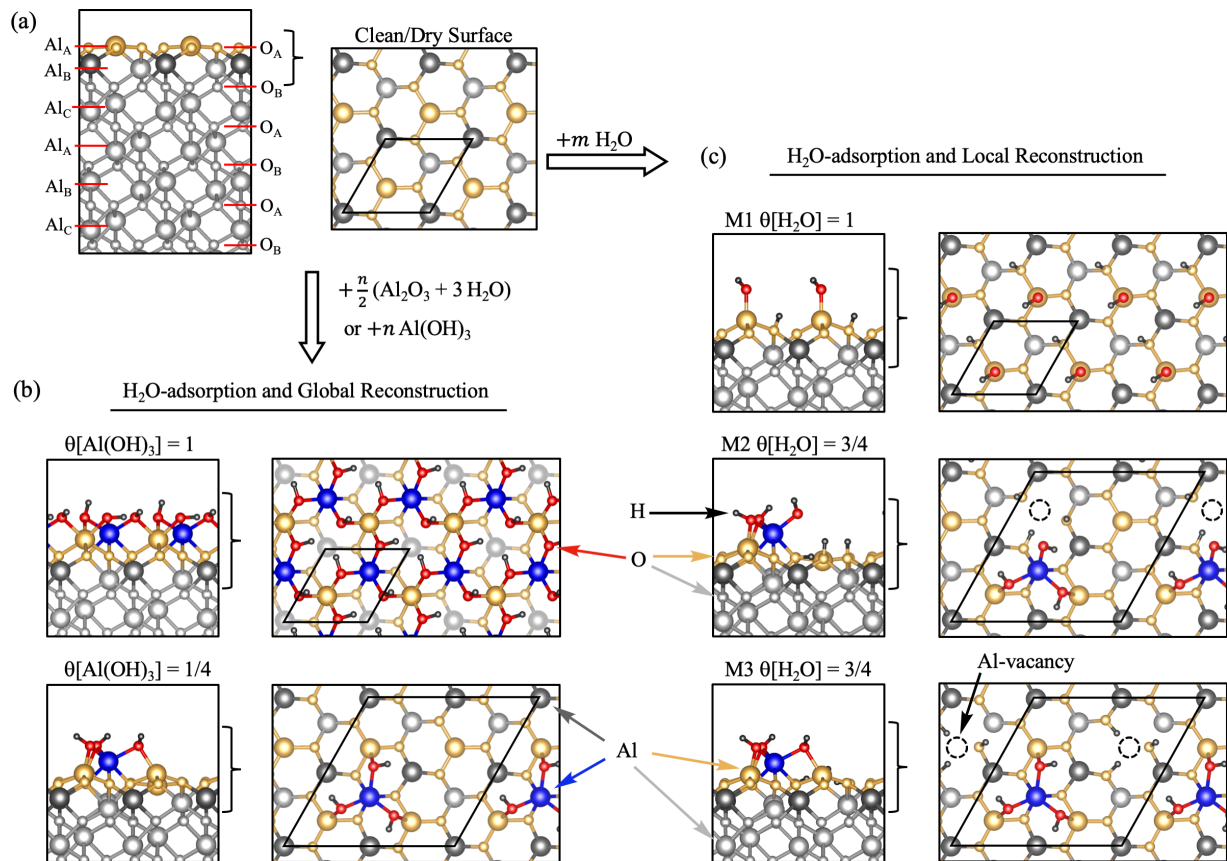


FIG. 1. Atomic structure of the most relevant surface terminations of α - $\text{Al}_2\text{O}_3(0001)$. (a) Clean and dry surface. (b) Surfaces with $\theta[\text{Al}(\text{OH})_3] = 1$ and $\frac{1}{4}$, which require diffusion of additional Al^{3+} ions onto the clean 0001 surface. (c) Metastable surfaces M1–M3 that can be obtained by adsorption of water and local reconstruction. The unit cell is indicated in the top views. The number of layers visible in the top views is indicated with braces in the respective side views.

this fully hydroxylated structure with an additional adsorbed water overlayer [42], in agreement with our and previous calculations [66–68]. If one compares the terminations of the stoichiometric surface (O_3 -Al) and that of the fully hydroxylated surface (Al_2 - $(\text{OH})_3$), it is clear that these two surfaces always differ by $\frac{3}{2} \text{H}_2\text{O}$ and $\pm \frac{1}{2} \text{Al}_2\text{O}_3$. Therefore the fully hydroxylated surface can be described as $\text{Al}(\text{OH})_3$ adsorbed on the stoichiometric surface with a coverage of $\theta[\text{Al}(\text{OH})_3] = 1$.

Figure 1 also shows a type of surface revolving around the structural motif of an isolated $\text{Al}(\text{OH})_3$ fragment adsorbed on the stoichiometric surface. By isolated we mean that a surface Al of the underlying stoichiometric surface (shown in gold in Fig. 1) binds at most to one of the surface OH groups, which bridge to the adsorbed $\text{Al}(\text{OH})_3$ (shown in blue in Fig. 1). This can be contrasted to the known, fully hydroxylated surface with $\theta[\text{Al}(\text{OH})_3] = 1$, where each surface Al binds to three OH groups. Importantly, the adsorbed $\text{Al}(\text{OH})_3$ binds in the position expected from the bulk structure of α - Al_2O_3 , and binding in the other available octahedral site is significantly weaker by 0.78 eV. The most stable orientation of the hydroxyl groups in the $\text{Al}(\text{OH})_3$ groups (clockwise or counterclockwise) depends on the relative orientation of oxygens in the lower layer. The difference in stability between the two different orientations is relatively large with 0.52 eV. This can be compared with the orientation of the hydroxyl groups in

the fully hydroxylated surface ($\theta[\text{Al}(\text{OH})_3] = 1$), where it has been shown that different configurations exist [75,93–96], in which individual hydroxyl groups can be orientated parallel to the surface to form hydrogen bonds, or point away from the surface. Here, we found very small differences of less than 0.01 eV per (1×1) unit cell.

Figure 2(a) shows the stability of the investigated surfaces as a function of the chemical potential of water, $\mu_{\text{H}_2\text{O}}$. At high values of $\mu_{\text{H}_2\text{O}}$, the fully hydroxylated surface $\theta[\text{Al}(\text{OH})_3] = 1$ is most stable, for $\mu_{\text{H}_2\text{O}} \geq -0.76$ with an additional 2D-ice-like overlayer of water (labeled H_2O^* in Fig. 2). Isolated $\text{Al}(\text{OH})_3$ groups can be formed up to a maximum coverage of $\theta[\text{Al}(\text{OH})_3] = \frac{1}{3}$, as illustrated in Fig. 2(b). Figure 2(a) shows that these surfaces become more stable than the fully hydroxylated surface already for $\mu_{\text{H}_2\text{O}} \leq -1.25$ eV, for example, at 500 K and 1 mbar H_2O pressure. Importantly, dehydroxylation and the formation of the clean stoichiometric surface are predicted only at $\mu_{\text{H}_2\text{O}} \leq -2.8$ eV, which is realized, for example, at around 1000 K and 1 mbar H_2O pressure or at 850 K and 0.001 mbar H_2O pressure; see Fig. 2(c). Complete dehydroxylation is therefore expected only for temperatures that are about 400 K higher than previously expected for the fully hydroxylated surface.

Isolated $\text{Al}(\text{OH})_3$ fragments show weakly repulsive adsorbate-adsorbate interaction for $\theta[\text{Al}(\text{OH})_3] \leq \frac{1}{3}$, leading to a systematic decrease in $\theta[\text{Al}(\text{OH})_3]$ from its maximum

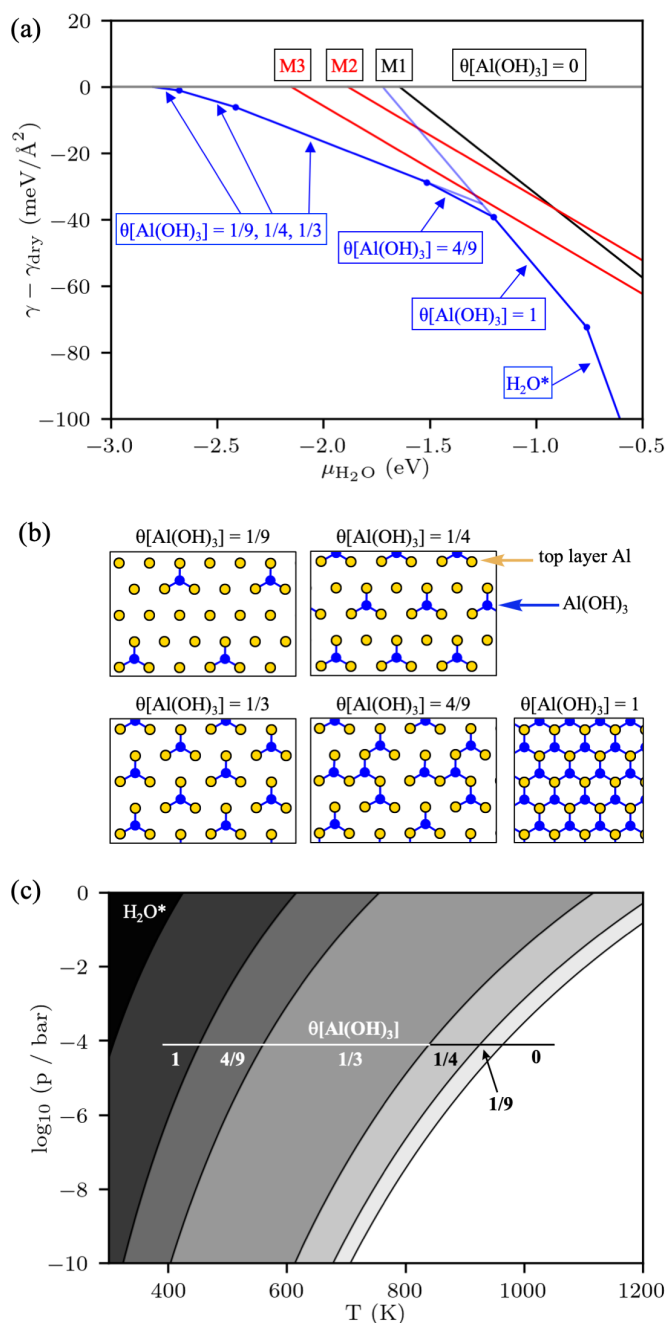


FIG. 2. Stability of α - $\text{Al}_2\text{O}_3(0001)$ surfaces. (a) Surface free energies, given relative to the dry surface as a function of the chemical potential of water $\mu_{\text{H}_2\text{O}}$. The most stable surfaces are shown in blue for various coverages $\theta[\text{Al}(\text{OH})_3]$. The metastable structures M1–M3 are shown in red and black. (b) Schematic representation of the surface Al configurations for the various coverages $\theta[\text{Al}(\text{OH})_3]$. (c) Phase diagram, showing only the most stable structures according to Eq. (1), where $\mu_{\text{H}_2\text{O}}$ was calculated using the rigid rotor and free translator approximation. At high chemical potentials of water, the most stable structure is a 2D-ice layer adsorbed on $\theta[\text{Al}(\text{OH})_3] = 1$, which is labeled H_2O^* .

value of $\frac{1}{3}$ to zero with increasing temperature and decreasing pressure, as shown in Fig. 2(c). As shown in Table I, the formation energy per water molecule increases only by 0.07 eV,

when going from $\frac{1}{3}$ to $\frac{1}{4}$ and then to $\frac{1}{9}$ coverage, illustrating the weak interaction. The difference in formation energy between $\frac{1}{9}$ and $\frac{1}{16}$ coverage is < 0.01 eV at the PBE-D3 level of theory, showing that adsorbate-adsorbate interaction is already negligible at $\theta[\text{Al}(\text{OH})_3] = \frac{1}{9}$. Table I also lists results obtained with other functionals as single-point energies based on the structure obtained with PBE-D3. These results show that the overall trends are the same; however, there is a general difference in the predicted stability of the hydroxylated surfaces with respect to the dry surface, where formation energies increase in the order $\text{SCAN} < \text{PBE-D3} < \text{BEEF-vdW} \lesssim \text{HSE06}$, i.e., SCAN predicts hydroxylated surfaces to be most stable (see also Fig. S2 of the Supplemental Material [88]).

The stability of the surfaces with $\theta[\text{Al}(\text{OH})_3] = \frac{1}{3}, \frac{1}{4},$ and $\frac{1}{9}$ shown in Fig. 2 was computed for $(\sqrt{3} \times \sqrt{3})R30^\circ, (2 \times 2),$ and (3×3) surfaces; see Fig. 2(b). However, due to the weak interaction, different configurations with the same coverages were found to show only negligible differences in stability. For example, different configurations for $\theta[\text{Al}(\text{OH})_3] = \frac{1}{4}$ differ by less than $1 \text{ meV}/\text{\AA}^2$, or equivalently by less than 0.05 eV per $\text{Al}(\text{OH})_3$ fragment (see Supplemental Material [88]). In the range of $-1.5 \text{ eV} < \mu_{\text{H}_2\text{O}} < -1.2 \text{ eV}$, there is a large variety of structures with similar stability with $\frac{1}{3} < \theta[\text{Al}(\text{OH})_3] < 1$. The most stable of these surfaces with $\theta[\text{Al}(\text{OH})_3] = \frac{4}{9}$ is included in Fig. 2. As is shown in Fig. 2(b), this surface is intermediate between having isolated $\text{Al}(\text{OH})_3$ groups and being fully hydroxylated.

Our results suggest that hydroxylated surfaces with $\theta[\text{Al}(\text{OH})_3] < 1$ may exhibit no ordered structure, because different configurations at the same coverage $\theta[\text{Al}(\text{OH})_3]$ show only very small differences in energy and because of the slow diffusion of $\text{Al}(\text{OH})_3$ (*vide infra*). For this reason, we discuss the state of these surfaces in terms of the coverage $\theta[\text{Al}(\text{OH})_3]$ rather than a specific surface reconstruction such as (2×2) . The lack of an ordered hydroxylated structure for $\theta[\text{Al}(\text{OH})_3] < 1$ may explain why in LEED experiments below 900°C generally only a (1×1) pattern is observed, which, however, improves with increasing temperatures, concomitantly with the desorption of water [97].

Finally, we now discuss the limitations of our investigation of the thermodynamic stability of these surfaces. Most importantly, it is of course possible that more stable terminations, for example, with different composition, exist. Secondly, our study is limited by the choice of unit cell, which allows only a finite number of configurations. However, for isolated $\text{Al}(\text{OH})_3$ groups, our investigation showed that adsorbate-adsorbate interaction is negligible already at $\theta[\text{Al}(\text{OH})_3] = 1/9$, since the formation energy changes by less than 0.01 eV when going from $\theta[\text{Al}(\text{OH})_3] = 1/16$ to $1/9$. Additionally, we have found that, for a given coverage $\theta[\text{Al}(\text{OH})_3]$, the stability does not depend strongly on the relative spatial positions of the $\text{Al}(\text{OH})_3$ groups. Consequently, we do not expect that an energetically particularly stable configuration of isolated $\text{Al}(\text{OH})_3$ groups was missed due to the limited number of studied unit cells. Our study did not account for vibrational and configurational entropy on the surface and only considered the loss of entropy upon adsorption of water. This approximation is expected to generally underestimate the stability of the hydroxylated surfaces with

TABLE I. Overview of computed terminations of the α - $\text{Al}_2\text{O}_3(0001)$ surface. The composition is specified in terms of the coverage of H_2O and $\text{Al}(\text{OH})_3$ adsorbates relative to the dry surface. The formation energy is given per two OH groups in eV relative to the dry surface, and ΔE_{form} is thus equal to the chemical potential $\mu_{\text{H}_2\text{O}}$ at which the surface free energy is identical to that of the stoichiometric surface; see Eq. (S1). Additionally, the concentration of hydroxyl groups per surface area, the unit cell, and the employed k -point sampling are specified.

Surface	Coverage (θ)		ΔE_{form} per 2OH (eV)				$n(\text{OH})$ (1/nm ²)	Unit cell	k -points
	$\text{Al}(\text{OH})_3$	H_2O	PBE-D3	BEEF-vDW ^a	SCAN ^a	HSE06 ^a			
Dry	0	0	0	0	0	0	0	b	b
$\theta[\text{Al}(\text{OH})_3] = 1/16$	1/16	0	-2.80	-2.75	-2.98	-2.76	0.9	(4 × 4)	1 × 1
$\theta[\text{Al}(\text{OH})_3] = 1/9$	1/9	0	-2.80	-2.75	-2.96	-2.74	1.7	(3 × 3)	2 × 2 ^c
$\theta[\text{Al}(\text{OH})_3] = 1/4$	1/4	0	-2.73	-2.70	-2.89	-2.67	3.8	(2 × 2)	2 × 2
$\theta[\text{Al}(\text{OH})_3] = 1/3$	1/3	0	-2.66	-2.66	-2.81	-2.58	5.0	($\sqrt{3} \times \sqrt{3}$)R30°	4 × 4 ^c
$\theta[\text{Al}(\text{OH})_3] = 4/9$	4/9	0	-2.37	-2.30	-2.51	-2.28	6.7	(3 × 3)	2 × 2 ^c
$\theta[\text{Al}(\text{OH})_3] = 1$	1	0	-1.72	-1.44	-1.87	-1.56	15.1	(1 × 1)	4 × 4
$\theta[\text{Al}(\text{OH})_3] = 1; \theta[\text{H}_2\text{O}] = 2$	1	2	-1.17	-0.93	-1.21	-0.99	35.3	(1 × 2)	4 × 2
M1	0	1	-1.64	-1.57	-1.71	-1.52	10.1	(1 × 1)	4 × 4
M2	0	3/4	-1.88	-1.73	-2.00	-1.77	7.6	(2 × 2)	2 × 2
M3	0	3/4	-2.15	-2.01	-2.31	-2.04	7.6	(2 × 2)	2 × 2

^aSingle-point calculation with the PBE-D3 structure.

^bThe dry surface serves as the reference and was always computed with the same unit cell and k -point sampling as the hydroxylated surfaces.

^cFor HSE06, the k -point sampling in each dimension was reduced by a factor of 2.

respect to the clean surface, especially at higher temperatures. We have studied four different density functionals, including a hybrid functional, which all support the main conclusion that the type of termination proposed herein is stable at low chemical potentials of water and that $\theta[\text{Al}(\text{OH})_3]$ is expected to decrease gradually with increasing temperature. However, the functionals differ in the prediction of the total stability of these surfaces and in the precise values of $\mu_{\text{H}_2\text{O}}$ at which the transitions between these terminations occur. The level of electronic structure theory could be improved, for example, with wave function methods that have already been applied to similar problems [69,74].

B. Kinetics and mechanism for the hydroxylation of the stoichiometric surface through local reconstruction

The hydroxylated structures discussed so far all have in common that they cannot be generated from the clean surface, without global reconstruction involving diffusion of additional Al^{3+} ions onto or away from the given 0001 facet. This has already been discussed for the fully hydroxylated surface $\theta[\text{Al}(\text{OH})_3] = 1$ [66,68]. Apart from the most stable, fully hydroxylated structure, previous theoretical investigations also studied hydroxylation starting from the initial adsorption of water on the clean surface, which dissociates with low barriers, < 0.5 eV [67,70]. At a coverage of $\theta[\text{H}_2\text{O}] = 1$, this leads to structure M1 in Fig. 1, which is metastable since it is always less stable than a structure with adsorbed $\text{Al}(\text{OH})_3$. Figure 1 shows that the structural motif of an isolated $\text{Al}(\text{OH})_3$ group can also be formed through local reconstruction. In structure M3, an Al vacancy is formed and saturated with three OH groups, and the removed Al^{3+} ion is placed on the surface as an adsorbed $\text{Al}(\text{OH})_3$ group in the same manner as for the structure with $\theta[\text{Al}(\text{OH})_3] = 1/4$. Importantly, formation of M3 from the clean surface involves only local reconstruction of the surface and the reaction with three H_2O molecules. Structure M3 can be described as a local coexis-

tence of 25% of the $\theta[\text{Al}(\text{OH})_3] = 1$ structure and 75% of the $\theta[\text{Al}(\text{OH})_3] = 1/3$ structure, and its stability is in fact almost identical to that of the linear combination of these surfaces. This is apparent from Fig. 2(a), which shows that the surface free energies of M3, $\theta[\text{Al}(\text{OH})_3] = 1/3$ and $\theta[\text{Al}(\text{OH})_3] = 1$, cross almost in one point, at $\mu_{\text{H}_2\text{O}} = -1.25$ eV. At $\mu_{\text{H}_2\text{O}} < -1.25$ eV, M3 is actually more stable than the fully hydroxylated surface, $\theta[\text{Al}(\text{OH})_3] = 1$.

We investigated the formation of structure M3 from the clean surface via water adsorption and dissociation to M1 followed by diffusion of Al^{3+} ions over the surface to form M3; see Fig. 3. A complete reaction pathway was obtained, for which all minima and transition states along the reaction pathway were computed [85–87]. Although M1 and M3 are (2 × 2)-surface structures, the path was computed for a (3 × 3) cell on which only four water molecules were adsorbed in the (2 × 2) area, where the reaction takes place. This approach was taken to avoid artificial interaction between periodic images of the surface reactions taking place, which would necessarily occur when using a (2 × 2) cell. We decided to start from only four adsorbed water molecules and leave the remaining five sites clean, mainly because this results in a less complex model and because we do not expect a large effect from additional coadsorbed water.

The most favorable pathway for the formation of structure M3 from structure M1 was found to proceed via two distinct Al migrations. In a first step, the $\text{Al}(\text{OH})_3$ moiety is formed through migration of the closest surface $\text{Al}(\text{OH})$ out of its initial position in the first layer (shown in gold) into the adsorbed position (shown in blue). After a few reaction steps, this gives the intermediate M2, also shown in Fig. 1. In a second Al migration, the Al vacancy is then moved farther away to give M3. In addition to water adsorption and dissociation, the reaction path involves 14 elementary reactions that include both H- and Al-diffusion steps. For one of the proton transfer steps, an adsorbed H_2O molecule was found to facilitate this process

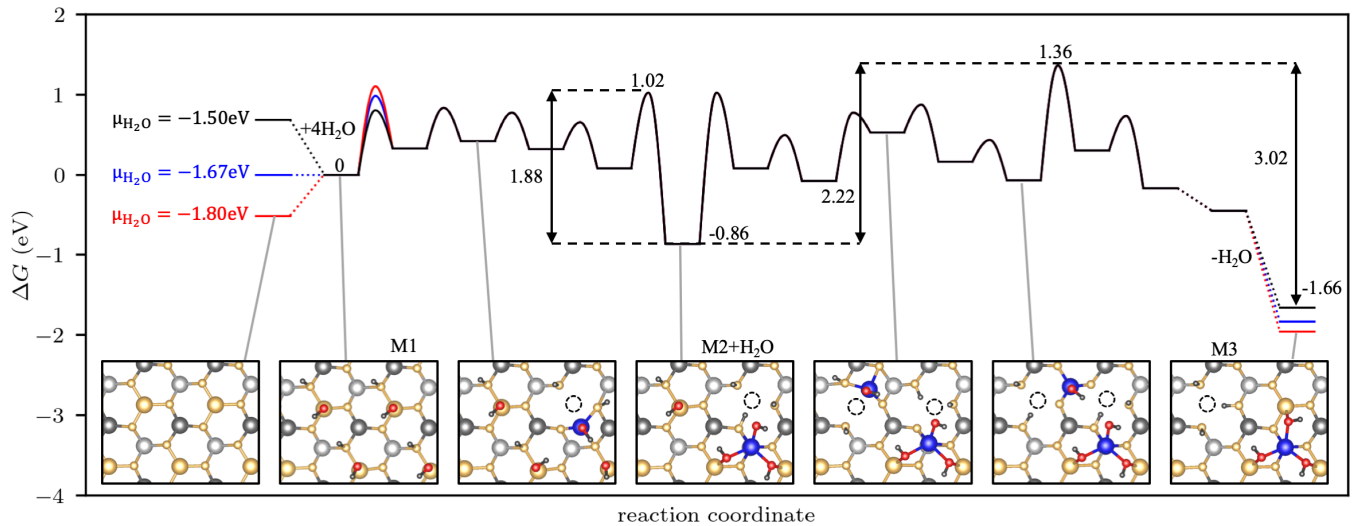


FIG. 3. Gibbs free energy diagram at $\mu_{\text{H}_2\text{O}} = -1.80$, -1.67 , and -1.50 eV for the reconstruction of structure M1 via structure M2 to structure M3. Calculations were performed for a (3×3) unit cell. Selected structures are shown as insets, with the same color code as in Fig. 1.

as a proton shuttle, which leads to the visible dependence of the corresponding barrier on the chemical potential of water. For all other proton transfers, where this was tested, additional water was not found to lower the barrier at relevant values of $\mu_{\text{H}_2\text{O}}$ for entropic reasons.

Figure 3 shows the free energy diagram for the transformation from M1 to M3 for different chemical potentials of water. The chosen values of $\mu_{\text{H}_2\text{O}} = -1.80$, -1.67 , and -1.50 eV were selected to illustrate the effect of $\mu_{\text{H}_2\text{O}}$ on the Gibbs free energy profile. At $\mu_{\text{H}_2\text{O}} = -1.67$ eV, the initial adsorption of the four H_2O molecules is thermoneutral, while it is uphill in free energy for smaller values of $\mu_{\text{H}_2\text{O}}$. The kinetics for the initial steps of reconstruction therefore depend on $\mu_{\text{H}_2\text{O}}$ and will become slower with decreasing $\mu_{\text{H}_2\text{O}} < -1.67$ eV, even if the formation of M3 is still favorable. We note that the value of $\mu_{\text{H}_2\text{O}} = -1.67$ eV, at which the adsorption of the four water molecules on the (3×3) surface ($\theta[\text{H}_2\text{O}] = \frac{4}{9}$) is thermoneutral, is slightly lower than the corresponding value of -1.64 eV given in Table I for $\theta[\text{H}_2\text{O}] = 1$, which we attribute to adsorbate-adsorbate interaction.

Starting from dissociatively adsorbed water, formation of M2 occurs with moderate barriers of up to 1.02 eV, which are accessible already at ambient temperatures. Importantly, M2 is already more stable than M1 for $\mu_{\text{H}_2\text{O}} < -0.90$ eV. We note that the type of reconstruction shown for M2 can also occur with a coverage of $1/3$, which is slightly more favorable (see Supplemental Material [88]). Due to the relatively high stability of M2, both the reaction backwards to M1 or forwards to M3 is associated with barriers of the order of 2 eV. This becomes feasible approximately at temperatures higher than 700 K, where a first-order rate constant with a barrier of 2.00 eV is 0.06 s^{-1} . Figure 3 shows that the decomposition of M3 to M1 is associated with a large barrier of 3.02 eV. It is important to note that the decomposition of M3 back to M1 and eventually to the clean surface also requires an additional water molecule, which facilitates the migration of the Al species. This results in a high kinetic stability of this surface, especially if water pressure is low, such as in

experiments where these surfaces were annealed in UHV and hydroxyl groups were still present [34,35].

C. Formation of extended hydroxylated surfaces

The formation of the extended surfaces listed in Figs. 1 and 2 with $\theta[\text{Al}(\text{OH})_3] = 1, \frac{4}{9}, \frac{1}{3}, \frac{1}{4}, \frac{1}{9},$ and $\frac{1}{16}$ requires the diffusion of additional Al onto the dry surface. The simplest mechanism for this is through direct diffusion of adsorbed $\text{Al}(\text{OH})_3$ over the stoichiometric surface; see Fig. 4. This is associated with a high barrier of 3.22 eV, which becomes feasible at temperatures around 1100 K, where a first-order rate constant with a barrier of 3.22 eV is 0.04 s^{-1} .

An alternative to the diffusion of $\text{Al}(\text{OH})_3$ is a water-mediated Al-vacancy migration mechanism, shown in Fig. 5. In this mechanism, an OH-saturated Al vacancy is assumed to be present on the surface. As discussed above and shown in Fig. 3, these vacancies can be formed concomitantly with the $\text{Al}(\text{OH})_3$ groups through local reconstruction. Migration of the Al vacancy occurs through the diffusion of a surface Al out of its initial position onto the surface and then into the vacancy position. This is facile when a mobile

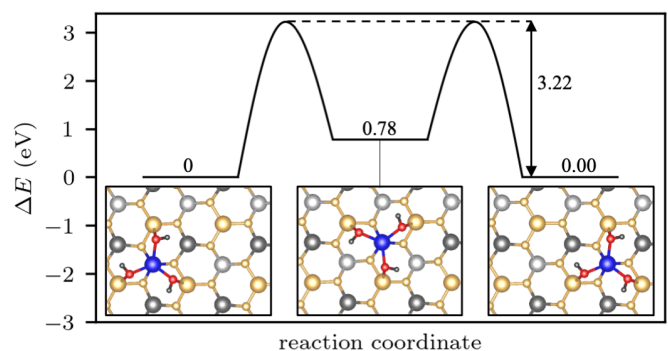


FIG. 4. Energy diagram for the diffusion of an adsorbed $\text{Al}(\text{OH})_3$ group. Calculations were performed for a (3×3) unit cell.

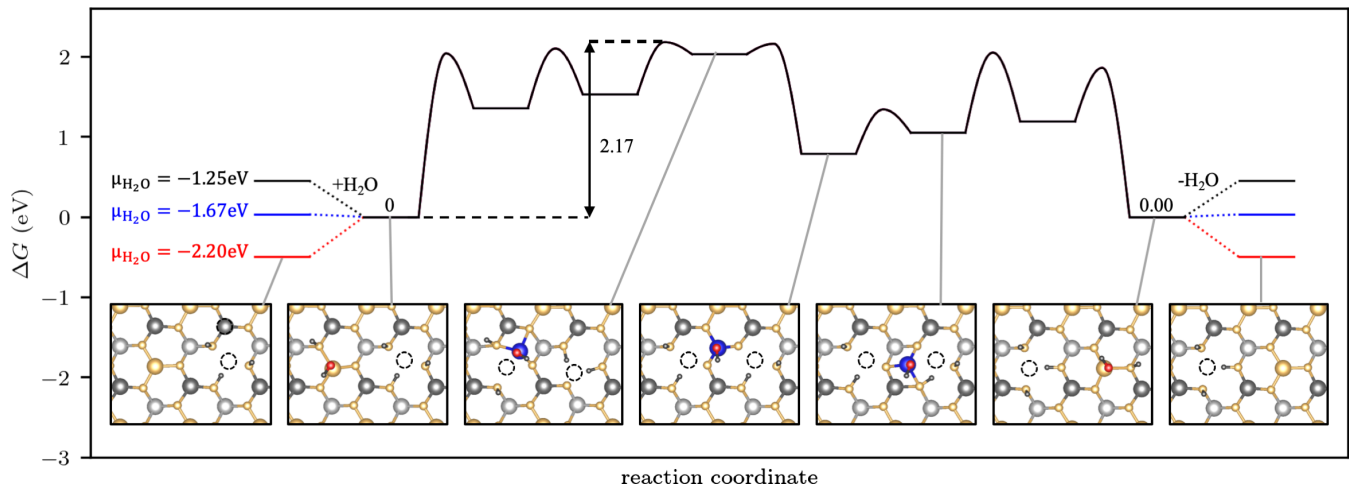


FIG. 5. Free energy diagram for the diffusion of an OH-saturated Al vacancy on the stoichiometric surface. The final state is in both cases equivalent to the initial state, with the $\text{Al}(\text{OH})_3$ group (Al vacancy) shifted right (left). Calculations were performed for a (3×3) unit cell. Selected structures are shown as insets, with the same color code as in Fig. 1.

$\text{Al}(\text{OH})$ species is created through dissociative H_2O adsorption. The mechanism for water-mediated Al-vacancy migration is thus similar to the transformation of M2 to M3 (Fig. 3), where an additional $\text{Al}(\text{OH})_3$ group is coadsorbed. The overall barriers are in both cases on the order of 2.2 eV. In contrast to migration of $\text{Al}(\text{OH})_3$, this mechanism requires the presence of an additional molecule of water and will become increasingly unfavorable, for $\mu_{\text{H}_2\text{O}} < -1.67$ eV. Similar to Fig. 3, Fig. 5 shows the Gibbs free energy diagram for different values of the chemical potential of water. The values of $\mu_{\text{H}_2\text{O}} = -2.20$, -1.67 , and -1.25 eV were chosen to illustrate how the Gibbs free energy surface changes when water adsorption becomes unfavorable thermodynamically.

Based on the reconstruction and diffusion mechanisms described above, one can now envision how the formation of extended hydroxylated $\alpha\text{-Al}_2\text{O}_3(0001)$ surfaces can take place. We have shown that, after adsorption and dissociation of water, local reconstruction can lead to a structure such as M3, which contains equal amounts of Al vacancies and adsorbed $\text{Al}(\text{OH})_3$. Redistribution of these species through diffusion allows the creation of extended facets of hydroxylated surfaces. Redistribution of $\text{Al}(\text{OH})_3$ adsorbed on the clean surface allows the formation of surfaces with $\theta[\text{Al}(\text{OH})_3] \leq 1$. Agglomeration of the corresponding OH-saturated Al vacancies exposes the underlying Al layer and thus leads to the formation of a lower lying, fully hydroxylated surface with $\theta[\text{Al}(\text{OH})_3] = 1$. This lower layer with $\theta[\text{Al}(\text{OH})_3] = 1$ could further rearrange itself into a structure with $\theta[\text{Al}(\text{OH})_3] < 1$ only through diffusion of Al^{3+} away from this facet. This would be possible via diffusion across a step edge, which was not investigated in this paper.

IV. CONCLUSION AND OUTLOOK

We have described a type of termination for the $\alpha\text{-Al}_2\text{O}_3(0001)$ surface that consists of isolated $\text{Al}(\text{OH})_3$ groups adsorbed on the dry surface. This termination is

predicted to be stable up to significantly higher temperatures than found in existing structural models for hydroxylated surfaces. Our investigation has shown that the interaction between adsorbed $\text{Al}(\text{OH})_3$ groups is only weakly repulsive for $\theta[\text{Al}(\text{OH})_3] \leq \frac{1}{3}$. Additionally, interaction at a given coverage shows only little dependence on the position of the adsorbates, which leads to many possible configurations with similar stability.

We have also investigated the formation and decomposition of hydroxylated surfaces, starting from the known pathway for adsorption and dissociation of water on the dry surface. Local reconstruction can then lead to the formation of adsorbed $\text{Al}(\text{OH})_3$ groups together with an equal amount of OH-saturated Al vacancies. The initial steps for reconstruction require only modest barriers of the order of 1 eV and already lead to surfaces that are more stable than the initial state, where water is dissociatively adsorbed. Further reconstruction towards the formation of the thermodynamically most stable surfaces requires barriers higher than 2 eV. The migration of Al atoms on the surface is generally facilitated by adsorbed water. Besides temperature, the kinetics for these processes are therefore also predicted to depend sensitively on the partial pressure of water. Importantly, this also applies to dehydroxylation, where the required surface reconstructions are also facilitated by water.

The hydroxylated terminations of the $\alpha\text{-Al}_2\text{O}_3(0001)$ surface proposed in this paper are predicted to be more stable than previously investigated structures over a wide range of the chemical potential of water. This will enable future studies on this surface to start from a more stable and appropriate structural model, depending on the specific conditions. Apart from the thermodynamic stability, we have computed reaction paths for the reconstruction and formation of these surfaces, which already allow a rough estimate of the kinetics of hydroxylation. A detailed prediction of the evolution of a given initial surface state for a certain temperature and partial pressure of water could be achieved with kinetic Monte Carlo simulations. Most of the information required for such

a simulation on a flat (0001) surface was computed in this paper; however, preexisting steps on such a surface could play an important role in the kinetics and were not considered. The hydroxylated structures found in this paper could also be relevant for other phases of Al_2O_3 and for other oxides that crystallize in the corundum structure, such as the oxides of Fe, Cr, and V, for which the hydroxylated 0001 surfaces have also been studied [98–106].

ACKNOWLEDGMENTS

The authors acknowledge support by the state of Baden-Württemberg through bwHPC (bwunicluster and JUSTUS, RV bw17D011). J.C. and P.N.P. acknowledge funding by Deutsche Forschungsgemeinschaft (DFG, German Research Foundation) - SFB 1441 - Project ID 426888090. Financial support from the Helmholtz Association is also gratefully acknowledged.

-
- [1] J. Feng, W. Zhang, and W. Jiang, *Ab initio* study of Ag/ Al_2O_3 and Au/ Al_2O_3 interfaces, *Phys. Rev. B* **72**, 115423 (2005).
- [2] J. D. Baran, H. Grönbeck, and A. Hellman, Mechanism for Limiting Thickness of Thin Oxide Films on Aluminum, *Phys. Rev. Lett.* **112**, 146103 (2014).
- [3] M. Koberidze, M. J. Puska, and R. M. Nieminen, Structural details of Al/ Al_2O_3 junctions and their role in the formation of electron tunnel barriers, *Phys. Rev. B* **97**, 195406 (2018).
- [4] J. Kang, J. Zhu, C. Curtis, D. Blake, G. Glatzmaier, Y.-H. Kim, and S.-H. Wei, Atomically Abrupt Liquid-Oxide Interface Stabilized by Self-Regulated Interfacial Defects: The Case of Al/ Al_2O_3 Interfaces, *Phys. Rev. Lett.* **108**, 226105 (2012).
- [5] G. Pilania, B. J. Thijssen, R. G. Hoagland, I. Lazić, S. M. Valone, and X.-Y. Liu, Revisiting the Al/ Al_2O_3 interface: Coherent interfaces and misfit accommodation, *Sci. Rep.* **4**, 4485 (2014).
- [6] W. Zhang and J. R. Smith, Nonstoichiometric Interfaces and Al_2O_3 Adhesion with Al and Ag, *Phys. Rev. Lett.* **85**, 3225 (2000).
- [7] D. J. Siegel, L. G. Hector, and J. B. Adams, Adhesion, atomic structure, and bonding at the Al(111)/ α - Al_2O_3 interface: A first principles study, *Phys. Rev. B* **65**, 085415 (2002).
- [8] Q. Zhang, T. Cagin, A. van Duin, W. A. Goddard, Y. Qi, and L. G. Hector, Adhesion and nonwetting-wetting transition in the Al/ α - Al_2O_3 interface, *Phys. Rev. B* **69**, 045423 (2004).
- [9] S. H. Oh, Y. Kauffmann, C. Scheu, W. D. Kaplan, and M. Rühle, Ordered liquid aluminum at the interface with sapphire, *Science* **310**, 661 (2005).
- [10] I. G. Batirev, A. Alavi, M. W. Finnis, and T. Deutsch, First-Principles Calculations of the Ideal Cleavage Energy of Bulk Niobium(111)/ α -Alumina(0001) Interfaces, *Phys. Rev. Lett.* **82**, 1510 (1999).
- [11] K. Shimamura, F. Shimojo, R. K. Kalia, A. Nakano, and P. Vashishta, Bonding and Structure of Ceramic-Ceramic Interfaces, *Phys. Rev. Lett.* **111**, 066103 (2013).
- [12] K. J. Harmon, K. Letchworth-Weaver, A. P. Gaiduk, F. Giberti, F. Gygi, M. K. Y. Chan, P. Fenter, and G. Galli, Validating first-principles molecular dynamics calculations of oxide/water interfaces with x-ray reflectivity data, *Phys. Rev. Mater.* **4**, 113805 (2020).
- [13] Y. R. Koh, J. Shi, B. Wang, R. Hu, H. Ahmad, S. Kerdsonpanya, E. Milosevic, W. A. Doolittle, D. Gall, Z. Tian, S. Graham, and P. E. Hopkins, Thermal boundary conductance across epitaxial metal/sapphire interfaces, *Phys. Rev. B* **102**, 205304 (2020).
- [14] C. Verdozzi, D. R. Jennison, P. A. Schultz, and M. P. Sears, Sapphire (0001) Surface, Clean and with *d*-Metal Overlayers, *Phys. Rev. Lett.* **82**, 799 (1999).
- [15] M. Trueba and S. P. Trasatti, γ -alumina as a support for catalysts: A review of fundamental aspects, *Eur. J. Inorg. Chem.* **2005**, 3393 (2005).
- [16] P. Christopher and S. Linic, Shape- and size-specific chemistry of Ag nanostructures in catalytic ethylene epoxidation, *ChemCatChem* **2**, 78 (2010).
- [17] M. García-Mota, M. Rieger, and K. Reuter, *Ab initio* prediction of the equilibrium shape of supported Ag nanoparticles on α - Al_2O_3 (0001), *J. Catal.* **321**, 1 (2015).
- [18] U. Hejral, P. Müller, O. Balmes, D. Pontoni, and A. Stierle, Tracking the shape-dependent sintering of platinum-rhodium model catalysts under operando conditions, *Nat. Commun.* **7**, 10964 (2016).
- [19] R. Molina and G. Poncelet, α -alumina-supported nickel catalysts prepared from nickel acetylacetonate: A TPR study, *J. Catal.* **173**, 257 (1998).
- [20] G. Poncelet, M. A. Centeno, and R. Molina, Characterization of reduced α -alumina-supported nickel catalysts by spectroscopic and chemisorption measurements, *Appl. Catal., A* **288**, 232 (2005).
- [21] Z. Hou, O. Yokota, T. Tanaka, and T. Yashima, Characterization of Ca-promoted Ni/ α - Al_2O_3 catalyst for CH_4 reforming with CO_2 , *Appl. Catal., A* **253**, 381 (2003).
- [22] M. Lyubovsky and L. Pfeifferle, Complete methane oxidation over Pd catalyst supported on α -alumina. Influence of temperature and oxygen pressure on the catalyst activity, *Catal. Today* **47**, 29 (1999).
- [23] F. Pompeo, N. N. Nichio, M. M. Souza, D. V. Cesar, O. A. Ferretti, and M. Schmal, Study of Ni and Pt catalysts supported on α - Al_2O_3 and ZrO_2 applied in methane reforming with CO_2 , *Appl. Catal., A* **316**, 175 (2007).
- [24] E. M. Dietze and P. N. Plessow, Predicting the strength of metal-support interaction with computational descriptors for adhesion energies, *J. Phys. Chem. C* **123**, 20443 (2019).
- [25] G. Sun, A. N. Alexandrova, and P. Sautet, Pt_8 cluster on alumina under a pressure of hydrogen: Support-dependent reconstruction from first-principles global optimization, *J. Chem. Phys.* **151**, 194703 (2019).
- [26] G. Li, B. Zandkarimi, A. C. Cass, T. J. Gorey, B. J. Allen, A. N. Alexandrova, and S. L. Anderson, Sn-modification of Pt_7 /alumina model catalysts: Suppression of carbon deposition and enhanced thermal stability, *J. Chem. Phys.* **152**, 024702 (2020).
- [27] T. Xie, B. J. Hare, P. J. Meza-Morales, C. Sievers, and R. B. Getman, Identification of the active sites in the dehydrogenation of methanol on Pt/ Al_2O_3 catalysts, *J. Phys. Chem. C* **124**, 19015 (2020).

- [28] Z. Łodziana and J. K. Nørskov, Adsorption of Cu and Pd on α -Al₂O₃(0001) surfaces with different stoichiometries, *J. Chem. Phys.* **115**, 11261 (2001).
- [29] I. Milas, B. Hinnemann, and E. A. Carter, Diffusion of Al, O, Pt, Hf, and Y atoms on α -Al₂O₃(0001): implications for the role of alloying elements in thermal barrier coatings, *J. Mater. Chem.* **21**, 1447 (2011).
- [30] B. Hinnemann and E. A. Carter, Adsorption of Al, O, Hf, Y, Pt, and S atoms on α -Al₂O₃(0001), *J. Phys. Chem. C* **111**, 7105 (2007).
- [31] N. J. O'Connor, A. S. M. Jonayat, M. J. Janik, and T. P. Senftle, Interaction trends between single metal atoms and oxide supports identified with density functional theory and statistical learning, *Nat. Catal.* **1**, 531 (2018).
- [32] L. Zhang, X. Fu, M. Hohage, P. Zeppenfeld, and L. D. Sun, Growth of pentacene on α -Al₂O₃(0001) studied by *in situ* optical spectroscopy, *Phys. Rev. Mater.* **1**, 043401 (2017).
- [33] J. Blomqvist and P. Salo, First-principles study for the adsorption of segments of BPA-PC on α -Al₂O₃(0001), *Phys. Rev. B* **84**, 153410 (2011).
- [34] C. Niu, K. Shepherd, D. Martini, J. Tong, J. A. Kelber, D. R. Jennison, and A. Bogicevic, Cu interactions with α -Al₂O₃(0001): effects of surface hydroxyl groups versus dehydroxylation by Ar-ion sputtering, *Surf. Sci.* **465**, 163 (2000).
- [35] R. Lazzari and J. Jupille, Wetting and interfacial chemistry of metallic films on the hydroxylated α -Al₂O₃(0001) surface, *Phys. Rev. B* **71**, 045409 (2005).
- [36] M. Messaykeh, J. Goniakowski, G. Cabailh, J. Jupille, R. Lazzari, P. Lagarde, and N. Trcera, Chromium adsorption reveals a persistent hydroxylation of vacuum-annealed α -Al₂O₃(0001), *J. Phys. Chem. C* **123**, 29245 (2019).
- [37] H.-L. Thi Le, R. Lazzari, J. Goniakowski, R. Cavallotti, S. Chenot, C. Noguera, J. Jupille, A. Koltsov, and J.-M. Mataigne, Tuning adhesion at metal/oxide interfaces by surface hydroxylation, *J. Phys. Chem. C* **121**, 11464 (2017).
- [38] R. Lazzari and J. Jupille, Chemical reaction via hydroxyl groups at the titanium/ α -Al₂O₃(0001) interface, *Surf. Sci.* **507-510**, 683 (2002).
- [39] X.-G. Wang, J. R. Smith, and M. Scheffler, Effect of hydrogen on Al₂O₃/Cu interfacial structure and adhesion, *Phys. Rev. B* **66**, 073411 (2002).
- [40] X. G. Wang, J. R. Smith, and M. Scheffler, Adhesion of copper and alumina from first principles, *J. Am. Ceram. Soc.* **86**, 696 (2003).
- [41] K. C. Hass, W. F. Schneider, A. Curioni, and W. Andreoni, The chemistry of water on alumina surfaces: Reaction dynamics from first principles, *Science* **282**, 265 (1998).
- [42] P. J. Eng, T. P. Trainor, G. E. Brown, G. A. Waychunas, M. Newville, S. R. Sutton, and M. L. Rivers, Structure of the hydrated α -Al₂O₃(0001) surface, *Science* **288**, 1029 (2000).
- [43] J. A. Kelber, Alumina surfaces and interfaces under non-ultrahigh vacuum conditions, *Surf. Sci. Rep.* **62**, 271 (2007).
- [44] C. C. Chang, LEED studies of the (0001) face of α -alumina, *J. Appl. Phys. (Melville, NY)* **39**, 5570 (1968).
- [45] T. M. French and G. A. Somorjai, Composition and surface structure of the (0001) face of α -alumina by low-energy electron diffraction, *J. Phys. Chem.* **74**, 2489 (1970).
- [46] G. Renaud, B. Villette, I. Vilfan, and A. Bourret, Atomic Structure of the α -Al₂O₃(0001)($\sqrt{31} \times \sqrt{31}$)R $\pm 9^\circ$ Reconstruction, *Phys. Rev. Lett.* **73**, 1825 (1994).
- [47] C. Barth and M. Reichling, Imaging the atomic arrangements on the high-temperature reconstructed α -Al₂O₃(0001) surface, *Nature (London)* **414**, 54 (2001).
- [48] E. A. A. Jarvis and E. A. Carter, Metallic character of the Al₂O₃(0001)-($\sqrt{31} \times \sqrt{31}$)R $\pm 9^\circ$ surface reconstruction, *J. Phys. Chem. B* **105**, 4045 (2001).
- [49] V. Coustet and J. Jupille, High-resolution electron-energy-loss spectroscopy of isolated hydroxyl groups on α -Al₂O₃(0001), *Surf. Sci.* **307-309**, 1161 (1994).
- [50] C. E. Nelson, J. W. Elam, M. A. Cameron, M. A. Tolbert, and S. M. George, Desorption of H₂O from a hydroxylated single-crystal α -Al₂O₃(0001) surface, *Surf. Sci.* **416**, 341 (1998).
- [51] Q. Fu, T. Wagner, and M. Rühle, Hydroxylated α -Al₂O₃(0001) surfaces and metal/ α -Al₂O₃(0001) interfaces, *Surf. Sci.* **600**, 4870 (2006).
- [52] J. Ahn and J. W. Rabalais, Composition and structure of the Al₂O₃{0001}-(1 \times 1) surface, *Surf. Sci.* **388**, 121 (1997).
- [53] J. W. Elam, C. E. Nelson, M. A. Cameron, M. A. Tolbert, and S. M. George, Adsorption of H₂O on a single-crystal α -Al₂O₃(0001) surface, *J. Phys. Chem. B* **102**, 7008 (1998).
- [54] J. Wirth, H. Kirsch, S. Wlosczyk, Y. Tong, P. Saalfank, and R. K. Campen, Characterization of water dissociation on α -Al₂O₃(1 $\bar{1}$ 02): theory and experiment, *Phys. Chem. Chem. Phys.* **18**, 14822 (2016).
- [55] T. Kurita, K. Uchida, and A. Oshiyama, Atomic and electronic structures of α -Al₂O₃ surfaces, *Phys. Rev. B* **82**, 155319 (2010).
- [56] T. Becker, A. Birkner, G. Witte, and C. Wöll, Microstructure of the α -Al₂O₃(11 $\bar{2}$ 0) surface, *Phys. Rev. B* **65**, 115401 (2002).
- [57] S. Aboud, J. Wilcox, and G. E. Brown, Density functional theory investigation of the interaction of water with α -Al₂O₃ and α -Fe₂O₃(1 $\bar{1}$ 02) surfaces: Implications for surface reactivity, *Phys. Rev. B* **83**, 125407 (2011).
- [58] A. Tougeri, C. Méthivier, S. Cristol, F. Tielens, M. Che, and X. Carrier, Structure of clean and hydrated α -Al₂O₃(1 $\bar{1}$ 02) surfaces: implication on surface charge, *Phys. Chem. Chem. Phys.* **13**, 6531 (2011).
- [59] S. Heiden, Y. Yue, H. Kirsch, J. Wirth, P. Saalfank, and R. Kramer Campen, Water dissociative adsorption on α -Al₂O₃(11 $\bar{2}$ 0) is controlled by surface site undercoordination, density, and topology, *J. Phys. Chem. C* **122**, 6573 (2018).
- [60] R. Wischert, P. Laurent, C. Copéret, F. Delbecq, and P. Sautet, γ -alumina: The essential and unexpected role of water for the structure, stability, and reactivity of "defect" sites, *J. Am. Chem. Soc.* **134**, 14430 (2012).
- [61] M. Digne, P. Sautet, P. Raybaud, P. Euzen, and H. Toulhoat, Hydroxyl groups on γ -alumina surfaces: A DFT study, *J. Catal.* **211**, 1 (2002).
- [62] M. Digne, P. Sautet, P. Raybaud, P. Euzen, and H. Toulhoat, Use of DFT to achieve a rational understanding of acid-basic properties of γ -alumina surfaces, *J. Catal.* **226**, 54 (2004).
- [63] Z. Łodziana, N. Y. Topsøe, and J. K. Nørskov, A negative surface energy for alumina, *Nat. Mater.* **3**, 289 (2004).
- [64] X. G. Wang, A. Chaka, and M. Scheffler, Effect of the Environment on α -Al₂O₃(0001) Surface Structures, *Phys. Rev. Lett.* **84**, 3650 (2000).
- [65] J. V. Lauritsen, M. C. R. Jensen, K. Venkataramani, B. Hinnemann, S. Helveg, B. S. Clausen, and F. Besenbacher,

- Atomic-Scale Structure and Stability of the $\sqrt{31} \times \sqrt{31}R9^\circ$ Surface of $\text{Al}_2\text{O}_3(0001)$, *Phys. Rev. Lett.* **103**, 076103 (2009).
- [66] V. A. Ranea, W. F. Schneider, and I. Carmichael, DFT characterization of coverage dependent molecular water adsorption modes on $\alpha\text{-Al}_2\text{O}_3(0001)$, *Surf. Sci.* **602**, 268 (2008).
- [67] V. A. Ranea, I. Carmichael, and W. F. Schneider, DFT investigation of intermediate steps in the hydrolysis of $\alpha\text{-Al}_2\text{O}_3(0001)$, *J. Phys. Chem. C* **113**, 2149 (2009).
- [68] P. Thissen, G. Grundmeier, S. Wippermann, and W. G. Schmidt, Water adsorption on the $\alpha\text{-Al}_2\text{O}_3(0001)$ surface, *Phys. Rev. B* **80**, 245403 (2009).
- [69] S. Heiden, D. Usvyat, and P. Saalfrank, Theoretical surface science beyond gradient-corrected density functional theory: Water at $\alpha\text{-Al}_2\text{O}_3(0001)$ as a case study, *J. Phys. Chem. C* **123**, 6675 (2019).
- [70] J. Wirth and P. Saalfrank, The chemistry of water on α -alumina: Kinetics and nuclear quantum effects from first principles, *J. Phys. Chem. C* **116**, 26829 (2012).
- [71] H. Kirsch, J. Wirth, Y. Tong, M. Wolf, P. Saalfrank, and R. K. Campen, Experimental characterization of unimolecular water dissociative adsorption on α -alumina, *J. Phys. Chem. C* **118**, 13623 (2014).
- [72] S. Heiden, J. Wirth, R. K. Campen, and P. Saalfrank, Water molecular beam scattering at $\alpha\text{-Al}_2\text{O}_3(0001)$: An *ab initio* molecular dynamics study, *J. Phys. Chem. C* **122**, 15494 (2018).
- [73] G. Melani, Y. Nagata, R. K. Campen, and P. Saalfrank, Vibrational spectra of dissociatively adsorbed D_2O on Al-terminated $\alpha\text{-Al}_2\text{O}_3(0001)$ surfaces from *ab initio* molecular dynamics, *J. Chem. Phys.* **150**, 244701 (2019).
- [74] T. Mullan, L. Maschio, P. Saalfrank, and D. Usvyat, Reaction barriers on non-conducting surfaces beyond periodic local MP2: Diffusion of hydrogen on $\alpha\text{-Al}_2\text{O}_3(0001)$ as a test case, *J. Chem. Phys.* **139**, 171103 (2022).
- [75] G. Melani, Y. Nagata, J. Wirth, and P. Saalfrank, Vibrational spectroscopy of hydroxylated $\alpha\text{-Al}_2\text{O}_3(0001)$ surfaces with and without water: An *ab initio* molecular dynamics study, *J. Chem. Phys.* **149**, 014707 (2018).
- [76] G. Melani, Y. Nagata, and P. Saalfrank, Vibrational energy relaxation of interfacial OH on a water-covered $\alpha\text{-Al}_2\text{O}_3(0001)$ surface: a non-equilibrium *ab initio* molecular dynamics study, *Phys. Chem. Chem. Phys.* **23**, 7714 (2021).
- [77] J. Sun, A. Ruzsinszky, and J. P. Perdew, Strongly Constrained and Appropriately Normed Semilocal Density Functional, *Phys. Rev. Lett.* **115**, 036402 (2015).
- [78] G. Kresse and D. Joubert, From ultrasoft pseudopotentials to the projector augmented-wave method, *Phys. Rev. B* **59**, 1758 (1999).
- [79] G. Kresse and J. Furthmüller, Efficient iterative schemes for *ab initio* total-energy calculations using a plane-wave basis set, *Phys. Rev. B* **54**, 11169 (1996).
- [80] J. P. Perdew, K. Burke, and M. Ernzerhof, Generalized Gradient Approximation Made Simple, *Phys. Rev. Lett.* **77**, 3865 (1996).
- [81] S. Grimme, J. Antony, S. Ehrlich, and H. Krieg, A consistent and accurate *ab initio* parametrization of density functional dispersion correction (DFT-D) for the 94 elements H-Pu, *J. Chem. Phys.* **132**, 154104 (2010).
- [82] J. Wellendorff, K. T. Lundgaard, A. Møgelhøj, V. Petzold, D. D. Landis, J. K. Nørskov, T. Bligaard, and K. W. Jacobsen, Density functionals for surface science: Exchange-correlation model development with Bayesian error estimation, *Phys. Rev. B* **85**, 235149 (2012).
- [83] J. Heyd, G. E. Scuseria, and M. Ernzerhof, Hybrid functionals based on a screened Coulomb potential, *J. Chem. Phys.* **118**, 8207 (2003).
- [84] A. V. Krukau, O. A. Vydrov, A. F. Izmaylov, and G. E. Scuseria, Influence of the exchange screening parameter on the performance of screened hybrid functionals, *J. Chem. Phys.* **125**, 224106 (2006).
- [85] P. N. Plessow, Efficient transition state optimization of periodic structures through automated relaxed potential energy surface scans, *J. Chem. Theory Comput.* **14**, 981 (2018).
- [86] G. Henkelman and H. Jónsson, A dimer method for finding saddle points on high dimensional potential surfaces using only first derivatives, *J. Chem. Phys.* **111**, 7010 (1999).
- [87] G. Henkelman and H. Jónsson, Improved tangent estimate in the nudged elastic band method for finding minimum energy paths and saddle points, *J. Chem. Phys.* **113**, 9978 (2000).
- [88] See Supplemental Material at <http://link.aps.org/supplemental/10.1103/PhysRevResearch.4.013232> for results with other density functionals, total energies, structures, and details regarding the investigated reaction paths.
- [89] Z. Łodziana, J. K. Nørskov, and P. Stoltze, The stability of the hydroxylated (0001) surface of $\alpha\text{-Al}_2\text{O}_3$, *J. Chem. Phys.* **118**, 11179 (2003).
- [90] I. Batyrev, A. Alavi, and M. W. Finnis, *Ab initio* calculations on the $\text{Al}_2\text{O}_3(0001)$ surface, *Faraday Discuss.* **114**, 33 (1999).
- [91] P. Guénard, G. Renaud, A. Barbier, and M. Gautier-Soyer, Determination of the $\alpha\text{-Al}_2\text{O}_3(0001)$ surface relaxation and termination by measurements of crystal truncation rods, *Surf. Rev. Lett.* **05**, 321 (1998).
- [92] G. Renaud, Oxide surfaces and metal/oxide interfaces studied by grazing incidence X-ray scattering, *Surf. Sci. Rep.* **32**, 5 (1998).
- [93] M. Dellostritto and J. Sofo, Bond polarizability model for sum frequency generation at the $\text{Al}_2\text{O}_3(0001)\text{-H}_2\text{O}$ interface, *J. Phys. Chem. A* **121**, 3045 (2017).
- [94] P. Huang, T. A. Pham, G. Galli, and E. Schwegler, Alumina(0001)/water interface: Structural properties and infrared spectra from first-principles molecular dynamics simulations, *J. Phys. Chem. C* **118**, 8944 (2014).
- [95] Y. Tong, J. Wirth, H. Kirsch, M. Wolf, P. Saalfrank, and R. K. Campen, Optically probing Al-O and O-H vibrations to characterize water adsorption and surface reconstruction on α -alumina: An experimental and theoretical study, *J. Chem. Phys.* **142**, 054704 (2015).
- [96] A. Sagara, H. Yabe, X. Chen, Y. Onabuta, S. Wang, M.-P. Gaigeot, M. Sprik, and M. Sulpizi, Oxide/water interfaces: how the surface chemistry modifies interfacial water properties, *J. Phys.: Condens. Matter* **24**, 124106 (2012).
- [97] P. S. P. Wei and A. W. Smith, Structure of the (0001) surface of α -alumina, *J. Vac. Sci. Technol.* **9**, 1209 (1972).
- [98] D. Costa, P. A. Garrain, B. Diawara, and P. Marcus, Biomolecule-biomaterial interaction: A DFT-D study of glycine adsorption and self-assembly on hydroxylated Cr_2O_3 surfaces, *Langmuir* **27**, 2747 (2011).
- [99] J. Schoiswohl, G. Tzvetkov, F. Pfuner, M. G. Ramsey, S. Surnev, and F. P. Netzer, Reactivity of $\text{V}_2\text{O}_5(0001)$ surfaces:

- Molecular vs dissociative adsorption of water, *Phys. Chem. Chem. Phys.* **8**, 1614 (2006).
- [100] A. Gouron, J. Kittel, T. De Bruin, and B. Diawara, Density functional theory study of monoethanolamine adsorption on hydroxylated Cr₂O₃ surfaces, *J. Phys. Chem. C* **119**, 22889 (2015).
- [101] S. Yamamoto, T. Kendelewicz, J. T. Newberg, G. Ketteler, D. E. Starr, E. R. Mysak, K. J. Andersson, H. Ogasawara, H. Bluhm, M. Salmeron, G. E. Brown, and A. Nilsson, Water adsorption on α -Fe₂O₃ (0001) at near ambient conditions, *J. Phys. Chem. C* **114**, 2256 (2010).
- [102] A. Hellman and R. G. Pala, First-principles study of photoinduced water-splitting on Fe₂O₃, *J. Phys. Chem. C* **115**, 12901 (2011).
- [103] X. Huang, S. K. Ramadugu, and S. E. Mason, Surface-specific DFT + *U* approach applied to α -Fe₂O₃(0001), *J. Phys. Chem. C* **120**, 4919 (2016).
- [104] M. H. Ahmed, X. Torrelles, J. P. Treacy, H. Hussain, C. Nicklin, P. L. Wincott, D. J. Vaughan, G. Thornton, and R. Lindsay, Geometry of α -Cr₂O₃(0001) as a function of H₂O partial pressure, *J. Phys. Chem. C* **119**, 21426 (2015).
- [105] S. M. Souvi, M. Badawi, J. F. Paul, S. Cristol, and L. Cantrel, A DFT study of the hematite surface state in the presence of H₂, H₂O and O₂, *Surf. Sci.* **610**, 7 (2013).
- [106] R. B. Wang and A. Hellman, Initial water adsorption on hematite (α -Fe₂O₃) (0001): A DFT + *U* study, *J. Chem. Phys.* **148**, 094705 (2018).